energies

MDPI

Article

Heat Transfer Calculations during Flow in Mini-Channels with Estimation of Temperature Uncertainty Measurements

Magdalena Piasecka [1,*], Beata Maciejewska [2] and Artur Piasecki [3]

[1] Faculty of Mechatronics and Mechanical Engineering, Kielce University of Technology, 25-314 Kielce, Poland
[2] Faculty of Management and Computer Modelling, Kielce University of Technology, 25-314 Kielce, Poland
[3] Echo Investment S.A., Al. Solidarności 36, 25-323 Kielce, Poland
* Correspondence: tmpmj@tu.kielce.pl; Tel.: +48-41-34-24-320

Abstract: The main aim of this work was to provide heat transfer calculations of flow boiling in mini-channels with an application for the Trefftz functions. The test section comprised five parallel mini-channels with a depth of 1 mm, with a common heated wall. For the estimation of the temperature uncertainty, during the experiment the temperature measurement was performed with the use of K-type thermoelements and an infrared camera in two mini-channels simultaneously. According to the *Guide to the Expression of Uncertainty in Measurement*, the Monte Carlo method is a practical alternative to the GUM uncertainty framework. Since the uncertainty components are not approximately the same magnitude, the Monte Carlo method was indicated to estimate the uncertainty of the surface temperature measurement. The results obtained from this simulation method were compared with the results of the computation related to the uncertainty propagation method. The results of both methods of temperature measurement were found to be consistent. The results of the statistical analysis were used to describe heat transfer calculations. The heat transfer investigations concerning the subcooled boiling region were performed during the other experiment. The local heat transfer coefficients on the contact surface between the working fluid and the heated wall were calculated from the Robin boundary condition. The mathematical model described by the heat equation in the mini-channel wall and by the Fourier-Kirchhoff equation in a flowing fluid leads to an inverse heat transfer problem. This problem was solved using the FEM with the Trefftz-type basis functions. The estimation of temperature uncertainty measurements due to the Monte Carlo method was included in the final results of the heat transfer coefficient.

Keywords: mini-channel; flow boiling; heat transfer coefficient; Trefftz functions; temperature measurement uncertainty; Monte Carlo method

Citation: Piasecka, M.; Maciejewska, B.; Piasecki, A. Heat Transfer Calculations during Flow in Mini-Channels with Estimation of Temperature Uncertainty Measurements. *Energies* **2023**, *16*, 1222. https://doi.org/10.3390/en16031222

Academic Editor: Frede Blaabjerg

Received: 4 January 2023
Revised: 18 January 2023
Accepted: 19 January 2023
Published: 23 January 2023

1. Introduction

Fluid flow mini- and micro-channels are widely used in many engineering applications, especially in compact heat exchangers. Different physical mechanisms occurred in heat and mass transport on the comparison of those processed at the macroscale with those in the microscale flow system. Heat transfer with change of phase, such as boiling during flow in channels, is of great interest in evaporator applications. Knowledge of the characteristics of heat transfer during boiling in small passages is needed to overcome the practical barriers associated with flow in such microscale channels. Flow boiling is being investigated considering heat removal from high-temperature-flux compact electronic devices and their components.

This article presents the results of investigations on boiling heat transfer during refrigerant flow in a set of five parallel mini-channels of 1 mm depth, asymmetrically heated by a common wall. The main purpose of the authors was to perform heat transfer calculations, including the estimation of temperature uncertainty measurements and other measurements related to the recording of the experiment data. The local heat transfer

coefficients on the contact surface between the working fluid and the heated wall were calculated using the 2D mathematical method from the Robin boundary condition. Furthermore, the uncertainty of surface temperature measurement was estimated using the Monte Carlo method. Temperature distributions on the heated surface of the examined wall surface were performed simultaneously using infrared thermography and K-type thermoelements during additional experiments. The temperature results were chosen for a comparative analysis. The solution of the heat transfer problem was performed due to mathematical methods based on Trefftz-type functions. In the heat transfer results, an estimate of uncertainties was included in the presentation of the final results.

In view of the fact that rapid technological growth and the demand for miniature devices require the intensification of the heat transfer process, a brief state-of-the-art review is presented below.

Various processes are tested for the manufacture of enhanced mini-channel heat exchangers, such as three-dimensional printing [1]. The application of a modified heater surface is widely studied as a method to increase the intensity of the boiling heat transfer process [2–4]. It should also be noted that it is not the only method that is seen to be a good way to increase heat exchange during flow. Heat transfer during refrigerant condensation in mini-channels is also investigated, as in [5–7]. Recently, the use of environmentally friendly refrigerants in industry has attracted particular attention [7].

The results of the experimental study carried out to investigate the heat transfer and fluid flow patterns during the boiling of propylene (R-1270) are presented in [1]. A small circular tube with a diameter of 1.0 mm was the essential element of the test section. The influence of heat flux, mass flux, vapor quality, and flow pattern on the heat transfer coefficient was analysed. It was noted that the heat transfer coefficient is highly dependent on heat and mass fluxes, and also on the vapor quality. The authors stated that the heat transfer coefficient increases with increasing vapor quality, mainly in the low vapor quality region (as the subcooled boiling region). The authors conducted a comparison of experimental results with some known empirical correlations, obtaining better or worse compliances for most data within the 35% error band.

The main aim of [2] was to investigate the impact of selected parameters on flow boiling heat transfer during the FC-72 flow in a set of mini-channels 1 mm deep. The mini-channels had a heated wall with a modified surface in contact with the fluid. Numerous types of enhanced surfaces were experienced, such as texturing by electro-machining and laser treatment, porous coatings with soldered iron powder, and formed by using emery papers. The authors noticed that the porous heated surface caused the highest temperature of the heated wall and, consequently, the lowest heat transfer coefficient. The application of electro-machining textured surfaces influences the reaching of the highest heat transfer coefficient, while the lowest coefficients were observed for the laser-textured heated wall. As a final result of the study, it was stated that specific microstructured surfaces with well-defined roughness, thermal flow parameters, and specific spatial orientation in the mini-channel heat exchanger could help to achieve heat transfer enhancement.

The authors of [7] investigated the feasibility of using metal three-dimensional printing as a manufacturing method to fabricate enhanced mini-channel heat exchangers. The single-phase thermal characteristics of an enhanced mini-channel heat exchanger equipped with longitudinal vortex generators were analysed both experimentally and numerically. Four different test sections, including a smooth channel as a benchmark, were printed via direct metal laser sintering technology for comparison. A test section was developed to test the prototypes under laminar flow conditions using distilled water as the working fluid. The experimental conditions were used as inputs for the numerical simulation using COMSOL software. One of the findings was that at the Reynolds number of about 1400 for one of the tested prototypes, the convective heat transfer resulted to be almost three times that of the smooth channel. The authors stated that additive manufacturing is a promising solution for the development of future enhanced mini-channel heat exchangers.

The results of experiments using a mini-gap test section were compared with a test section with a group of 50 parallel mini-channels and are discussed in [8]. Furthermore, the authors focused on investigating the modification of the mini-gap wall and found its influence on heat transfer intensification. The efficiency of heat transport and pressure drop depending on the system operating parameters was also analysed. Visualisations of flow patterns were provided and discussed.

Experimental and numerical heat transfer investigations in flow boiling of water through an asymmetrically heated, rectangular and horizontal mini-channel, with transparent side walls, were described in [9]. The recorded images of two-phase flow structures were analysed to calculate the void fraction. The laminar flows were investigated. In the mathematical model, the steady-state heat transfer process was assumed in the test section. Furthermore, two defined inverse heat transfer problems were solved with the help of the Trefftz method. One of the findings was that the heat transfer coefficient increased as the thickness of the mini-gap decreased. The heat transfer coefficient is also higher for a mini-channel multiport than for a mini-gap of the same cross-section area.

Experimental investigations of the effects of mass flux, heat flux and spatial orientation of the test section on the flow boiling of water and the critical heat flux characteristics were revealed by experiments described in [10]. The results showed that in mini-channel flow boiling, mass flux and heat flux had effects on the behaviour of vapour bubbles and consequently influenced the heat transfer coefficient. The spatial orientation of the test section has less effect on the heat transfer coefficient values. Furthermore, this factor affects the rate of forming and growing vapour bubbles.

The results of an experimental investigation into the water boiling heat transfer in a mini-channel flow are described in [11]. The test section was a circular mini-channel with a diameter of 2.12 mm, vertically oriented with the upward flow. The characteristics of heat transfer and fluid flow were studied. It was observed that the highest mass flux yielded the highest convective heat transfer coefficient. After analysing the vapour quality in contests of other parameters, it was noticed that, for the low vapour quality at a low flow rate, thin liquid film thermal evaporation becomes dominant, suggesting that thin liquid film thermal evaporation occurs at a lower heat flux.

Temperature measurement is a key issue for the technical diagnostics of device work, especially for an apparatus that generates large heat flux, including microelectronics with elements of a very high scale of integration. It is important to test the work of the compact heat exchangers considering the uncertainty of temperature measurement. Temperature measurements are usually complicated and costly. The use of advanced temperature measurement methods requires a large system to collect and process data. In addition, there is often the need to perform additional calibration procedures for temperature measurement. An example of such a technique for measuring the temperature of the solid surface is liquid crystal thermography, which requires colour calibration with respect to the corresponding temperature as a result of a calibration experiment [12,13]. Another method of contactless temperature measurement is infrared thermography. It allows temperature measurements to be made at a certain distance from the object. It is widely used because it is convenient for temperature measurement and is repeatable. There are numerous applications for infrared thermography, such as energy applications, construction, machine diagnostics, and medical diagnostics. It should be emphasized that the temperature measurement by an infrared camera is influenced by various factors such as the temperature of the ambient air and humidity, the distance from the object of which the temperature is measured, the lighting of the tested surface, and the correctly adjusted value of emissivity. Thermoelectric elements are broadly used because of their convenience and relatively low cost, which allows many sensors to contact the temperature measurement of the object/medium. Currently, thermoelements are applied in many industrial brands because of their wide range of temperatures and low costs. K-type thermoelements are characterised by commonly accepted measurement uncertainties. Moreover, to guarantee the higher accuracy of the measurements with thermoelements, additional calibration is needed. The authors of this

work have applied various methods of temperature measurement in flow boiling heat transfer research up to now. Recently, K-type thermoelements or infrared thermography [14] have been used to measure the temperature of the heated surface [15].

Among the many papers that have recently focused on heat transfer that are available in the literature, the results are based only on numerical simulations, for example, using the Laplace transform (as in [16]) or the Galerkin method (as in [17]). It should be emphasized that in this work, as well as in articles by other authors, such as [8,18–20], the results of the numerical calculations were based on their own experimental research.

The authors of this work continue their experimental and theoretical investigations, testing the application of analytical [2], semi-analytical-numerical methods with the application of the Trefftz functions [21–24] and several commercial numerical programs: Simcenter STAR-CCM+ [14], ADINA [25,26] and ANSYS CFX [27] programs to perform heat transfer calculations during fluid flow in mini-channels.

2. The Experimental Rig

2.1. Loops and Systems

Figure 1 illustrates the main elements of the main loops and systems, while the experimental devices were indicated as block schemes. The loops and systems are as follows: the flow loop with working fluid (FC-770), the data acquisition system and the power supply and control system. The basic devices of the flow loop are: a test section (1), a heat exchanger (2), a compensating tank (3), a filter (4), a gear pump (5), and a Proline Promass A 100 Endress-Hauser Coriolis mass flowmeter, (6). The PMP71 Cerabar S Endress-Hauser pressure meters, complement the system. An A655SC FLIR infrared camera, (7) recorded thermograms related to the measurement of the temperature distribution on the heater surface. A high-speed SP-5000M-CXP2 JAI video camera, helped to observe the flow structure during fluid flow (8). The supply and control system consists of an ammeter, a voltmeter (9), and an inverter welder heat source (10). The data acquisition system comprises data acquisition stations and a PC with the appropriate software (11).

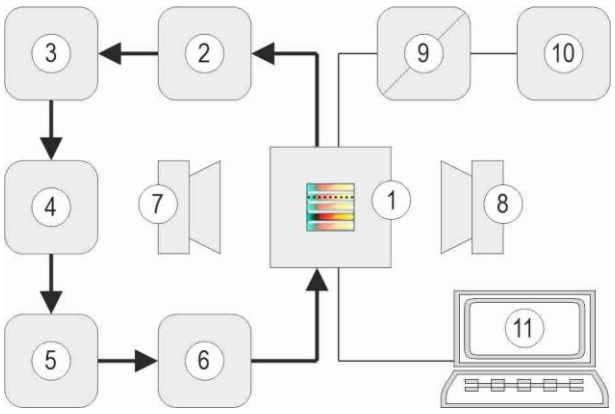

Figure 1. Block diagram of the main loops and systems realized on the experimental rig: (1) test section with mini-channels, (2) heat exchanger, (3) compensating tank, (4) filter, (5) circulating pump, (6) mass flow meter, (7) infrared camera, (8) high speed camera, (9) ammeter and voltmeter, (10) power supply, (11) data acquisition stations and PC computer.

2.2. Test Section

The test section is the essential element of the experimental rig. Diagrams of the test section are shown in Figure 2. A top view of the test section is shown in Figure 2a, while its longitudinal section is illustrated in Figure 2b. The working fluid was Fluorinert FC-770. The test section was vertically placed with upward flow. The front cover, Figure 2b, (1) and the body (2) were made of aluminium. In the Teflon spacer (4), five mini-channels were formed, each 1 mm deep and 6.8 mm wide. The length of each mini-channel corresponding

to the recorded temperature field was 32 mm. The heater for the working fluid (FC-770) flowing in the mini-channels was a Haynes-230 alloy foil (2), 0.04 inch thick. The temperature of the outer surface of the foil (in contact with ambient air) was measured using an infrared camera. The foil surface was covered with black paint with a known emission coefficient (0.98). The glass plate (5) allowed for observation of the flow structures. Pressure meters and K-type thermoelements were installed in the inlet and outlet chambers of the test section.

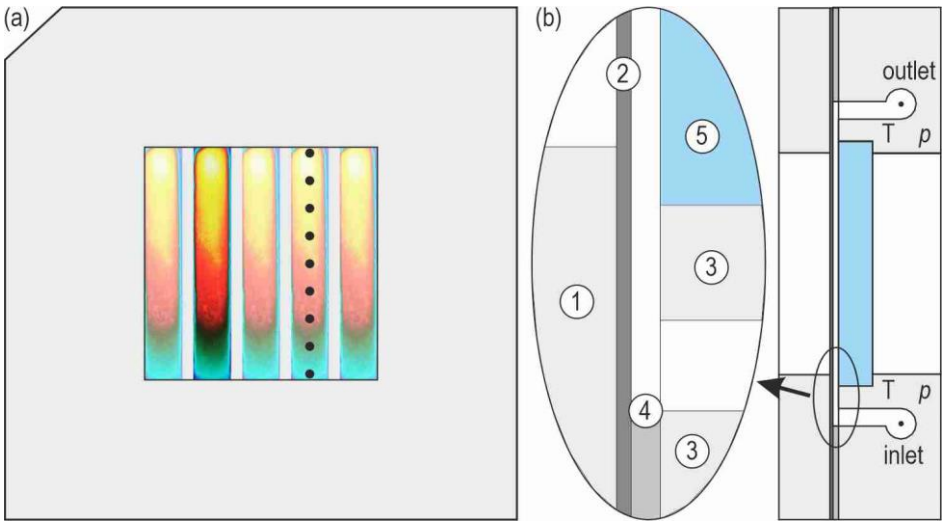

Figure 2. The test section with mini-channels: (**a**) view on the side of the front cover, (**b**) cross section along the mini-channels, (1) front cover, (2) heated foil, (3) body, (4) spacer with mini-channels, (5) glass plate, T-thermocouple, *p*–pressure measurement.

2.3. Temperature Measurement Apparatus

The following temperature measurement instruments were used in the experiments:

- The FLIR A655SC infrared camera used with FLIR ResearchIR Max software (v.4.4) to measure the temperature distribution on the surface.

  Main specifications of the FLIR A655SC infrared camera:

  - a spectral range of 7.5–14.0 μm,
  - a resolution of 640 × 480 pixels,
  - an accuracy of temperature measurement of 2% in the range of 0–120 °C or 2 °C.

  Furthermore, FLIR ResearchIR Max software allows for indicating the temperature at the points of thermograms.

- The thermoelements manufactured by Czaki Thermo-Product, Raszyn-Rybie, Poland, helped measure the temperature at selected points on the heated surface.

  Main specifications of the thermoelements:

  - NiCr-NiAl thermoelement: a K-type sheathed thermoelement sensor with an outer diameter of 0.5 mm, model TP-221,
  - a nominal range of temperature measurement from −40 °C to 600 °C,
  - a temperature sensor with a galvanically isolated weld (type b),
  - a wire length of 100 mm,
  - a temperature measurement accuracy of 1.5 °C according to international standards.

3. Experimental Procedures and Parameters

3.1. The Experiment for Estimation of Temperature Uncertainty Measurements

After deaeration, the temperature and flow parameters stabilized. The current of known intensity was supplied from the heat source (an inverter welder) to the heated wall of the mini-channels. It resulted in heat flux supplied to the heated foil. The temperature of the outer surface of the foil was measured as a result of the use of an infrared camera and thermoelements. Due to infrared thermography, temperature distributions on the entire heater surface temperature were obtained. Due to K-type thermoelements, the temperature was recorded at nine points spaced every 5 mm on the foil along the mini-channel axis. Measurements were taken with a time interval of 1/25 s. In the full experimental series, 400 readings were recorded over 16 s.

3.2. The Heat Transfer Experiment

The experimental procedure was similar to that described in Section 3.1; however, two stages of the procedure differ. After deaeration and stabilisation of the parameters, the heat flux supplied to the heater was increased. During the full experimental series, convective heat transfer was transferred to flow boiling. Measurements were taken with a 1 s time interval. Infrared thermography was chosen as the technique for temperature measurement on the heated foil's outer surface. The experiments were carried out under time-dependent conditions, while measurements were recorded with a time interval of 1 s. In the full experimental series, observation of the flow structures helped to control this process. The main parameters of the experimental series are listed in Table 1.

Table 1. The main experimental parameters for the heat transfer experiment.

Parameter	Value/Range
Heat Flux (entire experiment), q (kW/m^2)	4.9–63.7
Heat Flux (selected part of the experiment), q (kW/m^2)	36.7–49.8
Mass Flow Rate, (kg/s)	0.004
Inlet Pressure, (kPa)	118–167

4. Method of Estimation of Temperature Uncertainty Measurements

To estimate the uncertainty of the temperature measurement, the probability distribution of the output quantity was determined on the basis of the probability distributions assigned to the input quantities. The central mini-channel of the test section was considered as a model channel in future considerations.

The output quantity T considered using thermoelements for temperature measurement was determined according to Equation (1), and for infrared thermography according to Equation (2), as follows:

$$T_{TK} = \overline{T_{TK}} + \delta_{TK} + \delta_{DaqLab} \quad (1)$$

$$T_{IR} = \overline{T_{IR}} + \delta_{IR} \quad (2)$$

where: $\overline{T_i}$—the estimate of the temperature measurement obtained as the average value of the series of measurement results, $I = TK, IR$; δ_{TK}—the accuracy of K-type thermoelement given by the manufacturer, $\delta_{TK} = \pm 1.5$ °C, δ_{IR}—the accuracy of the infrared camera given by the manufacturer, $\delta_{IR} = \pm 2$ °C, δ_{DaqLab}—the accuracy of the DaqLab 2005 data acquisition station including the thermocouple card, $\delta_{DaqLab} = \pm 0.5$ °C.

The estimation of the uncertainty of temperature measurements using the Monte Carlo method was performed according to the recommendations formulated in [28].

The variance $u^2(\delta_i)$, $i = TK,\ IR$ was determined by assuming a normal probability distribution of δ_{TK} and δ_{IR}, according to the following equation:

$$u^2(\delta_i) = \left(\frac{\delta_i}{2}\right)^2, i = TK,\ IR \quad (3)$$

The variance $u^2(\delta_{DaqLab})$, was designed as follows:

$$u^2\left(\delta_{DaqLab}\right) = \left(\frac{\delta_{DaqLab}}{\sqrt{3}}\right)^2 \tag{4}$$

assuming a rectangular probability distribution of δ_{DaqLab}.

The normal probability distribution of $\overline{T_{TK}}$ and $\overline{T_{IR}}$ was assumed. Next, the variance $u^2(\overline{T_i})$, $i = TK,\ IR$ was determined from the formula:

$$u^2\left(\overline{T_i}\right) = \frac{1}{n(n-1)}\sum_{j=1}^{n}\left(T_i^j - \overline{T_i}\right)^2,\ i = TK,\ IR \tag{5}$$

where n—number of measurements.

The probability density functions (PDF) of the output quantities T_i, $i = TK,\ IR$ were calculated using the probability distributions based on Equations (1) and (2).

To determine the empirical cumulative distribution functions (eCDF) F_i, $i = TK,\ IR$ of the output quantities, the values of the output quantities $T_{i,r}$, $i = TK,\ IR,\ r = 1, \ldots, M$ obtained in the MC simulation were sorted.

The cumulative probability was then assigned to the sorting values of the output quantities in the following form:

$$p_{i,r} = \frac{r - \frac{1}{2}}{M},\ i = TK,\ IR,\ r = 1, \ldots, M \tag{6}$$

For each of the distributions defined by the empirical distribution of the output quantity $T_{TK,}\ T_{IR}$, quantiles of the order of 0.025 and 0.975 were determined, respectively. The values of these quantiles equal to ${F_i}^{-1}(0.025)$, ${F_i}^{-1}(0.975)$, $i = TK,\ IR$ are the extremes of the confidence intervals for the output quantities at the confidence level of 0.95 [28].

5. Determination of the Heat Transfer Coefficient

Local heat transfer coefficients α are calculated from the formula [13]:

$$\alpha(x,t) = \frac{-\lambda_F \frac{\partial T_F(x,\delta_F,t)}{\partial y}}{T_F(x,\delta_F,t) - T_{f,bulk}(x,t)} \tag{7}$$

where the foil (T_F) and fluid (T_f) temperature distributions were obtained as the results of the solutions of the inverse heat transfer problem described by the set of following differential equations [13]:

$$\kappa_F\ \nabla^2 T_F - \frac{\partial T_F}{\partial t} = -\frac{q(t)}{\delta_H \cdot \lambda_H} \text{ for } (x,y) \in \Omega_F,\ \ t > 0 \tag{8}$$

$$\kappa_f\ \nabla^2 T_f - v_x(y,t)\frac{\partial T_f}{\partial x} - \frac{\partial T_f}{\partial t} = 0 \text{ for } (x,y) \in \Omega_M,\ t > 0 \tag{9}$$

and the boundary conditions given in Figure 3.

The nomenclature referring to Equations (7)–(9) and the boundary conditions illustrated in Figure 3, are as follows:

x—coordinate consistent with the direction along the flow;

y—coordinate consistent with the mini-channel depth;

$T_{f,bulk}$—temperature in the flow core;

κ_F—thermal diffusivity coefficient of the heated foil, $\kappa_F = \frac{\lambda_F}{\rho_F\ c_{p,F}}$,

where

λ_F—thermal conductivity of the heated foil;

ρ_F- density of the heated foil;

$c_{p,F}$ —specific heat of the heated foil;

κ_f—thermal diffusivity coefficient of the working fluid, $\kappa_f = \frac{\lambda_f}{\rho_F \, c_{p,F}}$,
where
λ_f —thermal conductivity of the working fluid;
ρ_f—density of the working fluid;
$c_{p,f}$ —specific heat of the working fluid;
q—heat flux (density); $q(t) = \frac{I(t)\Delta U(t)}{A}$,
where
A—cross-sectional area of the heated foil;
I—the current supplied to the heated foil;
ΔU—the voltage drop across the heated foil;
$v_x(y,t)$—component of the fluid velocity vector;
T_{IR}—the temperature of the heated foil measured on its outer surface using an infrared camera;
$T_{f,in}$, $T_{f,out}$—the fluid temperature measured by K-type thermoelements at the inlet and outlet of the mini-channel.

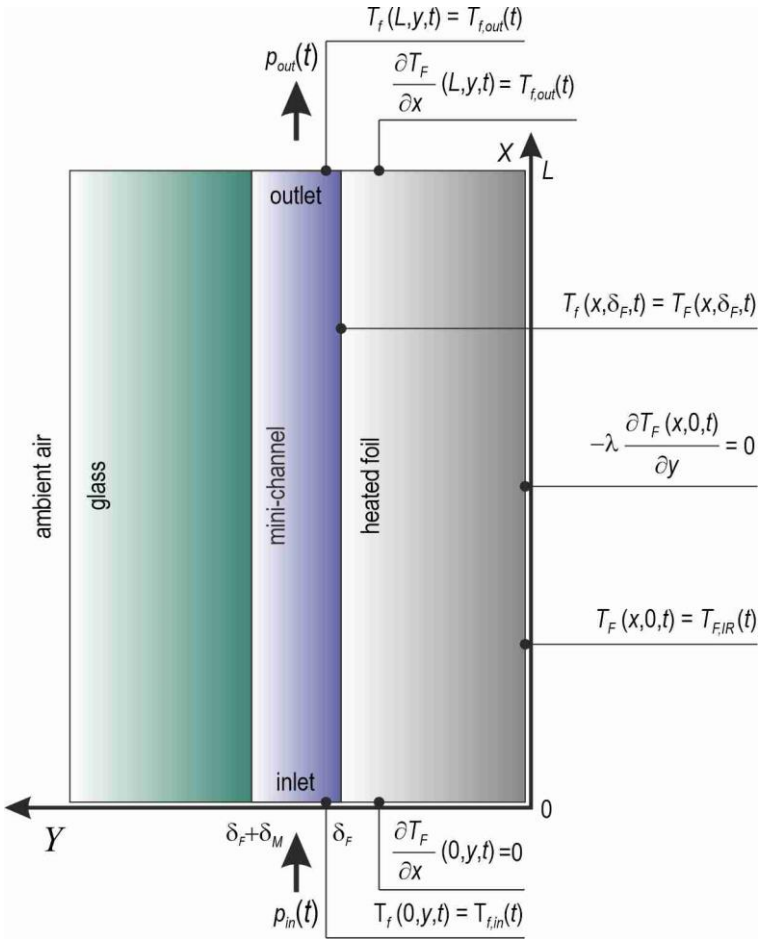

Figure 3. Boundary conditions.

Domains Ω_H and Ω_H are defined as follows:

$$\Omega_F = \left\{(x,y) \in R^2 : \; 0 \le x \le L, \; 0 \le y \le \delta_F \right\};$$

$$\Omega_M = \left\{(x,y) \in R^2 : 0 \le x \le L, \; \delta_F \le x \le \delta_F + \delta_M \right\}$$

where

L—length of the mini-channel,
δ_F —thickness of the heated foil,
δ_M —depth of the mini-channel.
The initial conditions have the following forms:

$$T_F(x, y, 0) = T_{IR}(x_i, 0) \tag{10}$$

$$T_f(x, y, 0) = T_{f,in}(0) \tag{11}$$

6. Presentation and Discussion of the Results

6.1. Estimation of Temperature Uncertainty Measurements

6.1.1. Experimental Outline

The experimental data recorded by an infrared camera and K-type thermoelements simultaneously were considered to estimate the temperature uncertainty measurements of the mini-channel heated wall surface. Example results obtained with the use of both measurement techniques are shown and discussed. A methodology of determining the uncertainty of surface temperature measurement with the use of the Monte Carlo method is proposed. A comparative analysis of the results obtained from the Monte Carlo simulation and the uncertainty propagation method is also performed, and their results are reported.

Temperature measurements, performed simultaneously in two mini-channels during the experiment, were taken into account in the analysis. The data were collected at the same selected distance from the inlet in two mini-channels on the central axis of the foil. The top view of the test section showing the mini-channels selected for statistical analysis of temperature measurement is illustrated in Figure 4. The points on the heated foil surface, regarding the place taken into consideration, are indicated. These points correspond to the axial position of two thermoelements: Nos. T_5 and T_8.

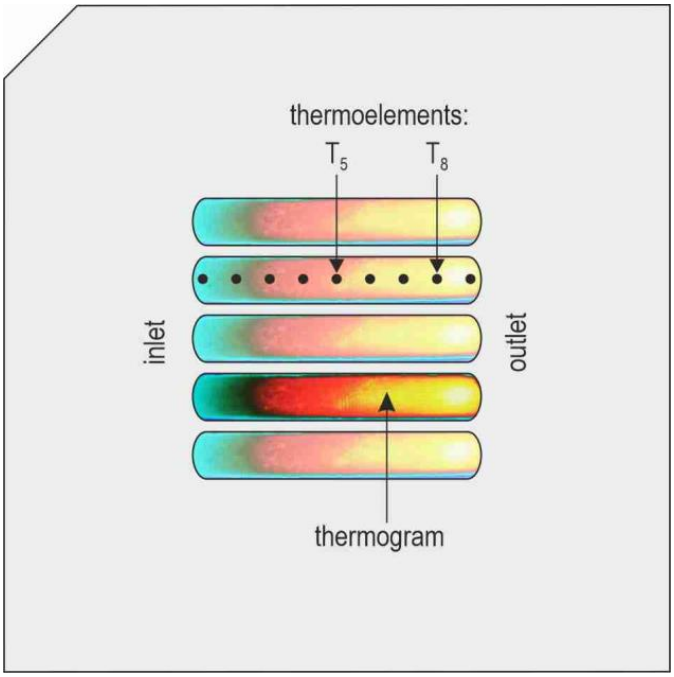

Figure 4. The test section–top view showing mini-channels selected for statistical analysis of temperature measurement data; the selected points for temperature measurement realized on the heated wall surface are indicated.

6.1.2. Experimental Data

Figure 5 shows the experimental results of the temperature measurements performed by the selected K-type thermoelements and the infrared camera, considering the same distance from the inlet. Data resulting from the analysis correspond to the positions of the thermoelements numbered 5 (Figure 5a) and 8 (Figure 5b). It should be emphasized that the measurements were performed simultaneously.

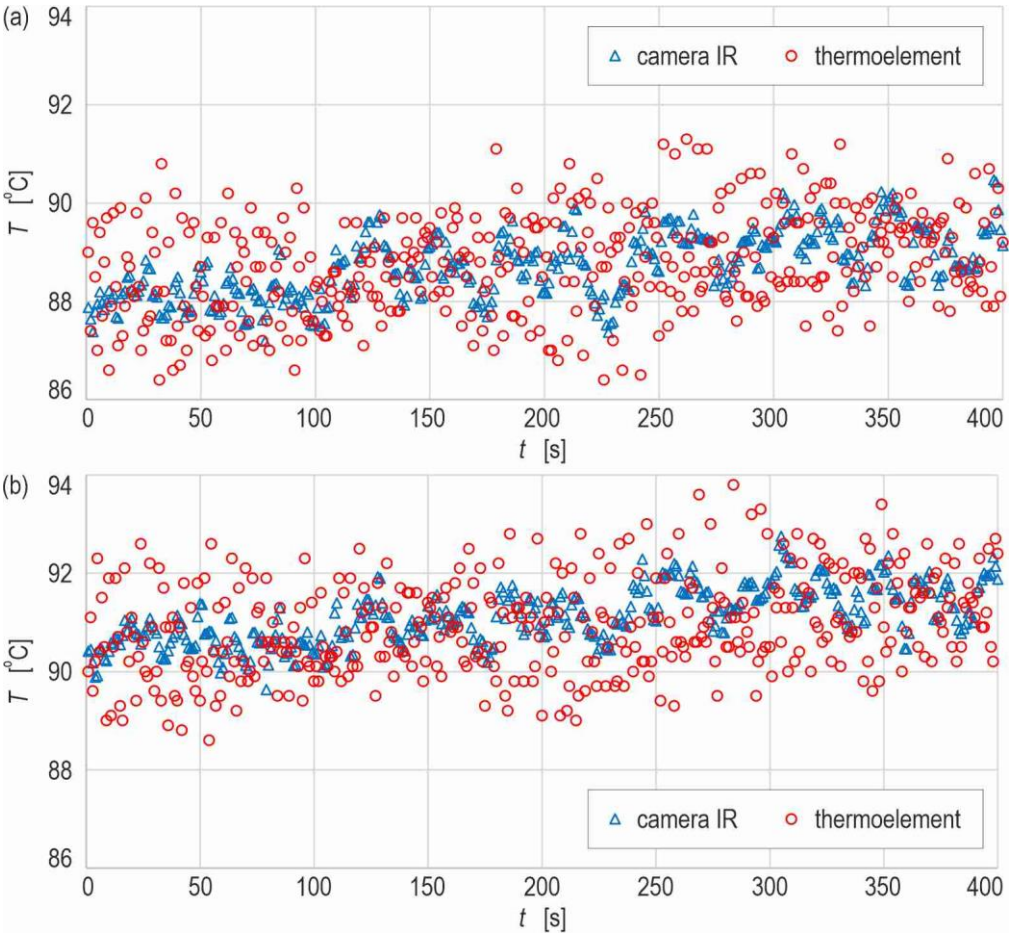

Figure 5. Temperature measurements performed by the thermoelements and the infrared camera, at the same distance from the inlet, corresponding to the thermoelement positions: Nos. 5 (**a**) and 8 (**b**).

6.1.3. Estimation of Temperature Measurement Uncertainty

The Monte Carlo method was used to estimate the uncertainty of temperature measurements recorded simultaneously with K-type thermoelements and due to infrared thermography. A value of M, the number of Monte Carlo trials, that is, the number of model evaluations to be made, was 10^6. The values of the input quantities and statistical parameters are listed in Table 2. Input quantities cover the average values of temperature measurements and the assumed accuracy of the K-type thermoelement, the infrared camera, and the data acquisition station.

Table 2. Values of input quantities and statistical parameters.

Input Quantity	Estimate of Input Quantity [°C]	Estimate of Input Quantity Variance [°C^2]	Estimate of Input Quantity Standard Variation [°C]
$\overline{T_{TK\_5}}$	88.75	0.00261	0.05108
$\overline{T_{TK,8}}$	90.92	0.00237	0.04872
$\overline{T_{IR\_5}}$	88.73	0.00109	0.03307
$\overline{T_{IR,8}}$	91.13	0.00081	0.02850
δ_{TK}	0	0.5625	0.75
δ_{IR}	0	1	1
δ_{DaqLab}	0	0.00083	0.02887

Based on the assumed probability distributions and variances described in Equations (3)–(5) and the values of the input parameters given in Table 2, the distributions of the output quantities T_i, $i = TK,\ IR$ were calculated according to Equations (1) and (2). Estimates of the output quantities as mean values of the results obtained in the MC simulations are shown in Table 3.

Table 3. Estimates of output quantities and expanded uncertainties of temperature measurements.

Output Quantity	Estimate of Output Quantity [°C]	Expanded Uncertainty	
		MC Simulation [28], U_{MC} [°C]	Uncertainty Propagation Method [29] U_{PM}, k = 2 [°C]
$T_{TK,5}$	88.75	1.47	1.50
$T_{TK,8}$	90.92	1.48	1.50
$T_{IR,5}$	88.73	1.97	2
$T_{IR,8}$	91.13	1.96	2

The confidence intervals (at a confidence level of 0.95) for the output quantities were symmetrical with respect to the mean of the simulation results. Therefore, only the quantile of 0.975 order (the right ends of the confidence intervals for the output) was considered. Expanded uncertainties obtained from the MC simulation according to the following formula

$$U_{MC} = F^{-1}\left(\frac{1+p}{2}\right) - T_j \tag{12}$$

were compared with the expanded uncertainties determined by the uncertainty propagation method [29]:

$$U_{PM} = k\sqrt{\sum_i {u_i}^2} \tag{13}$$

where p—confidence level, p = 0.95, T_j—estimates of output quantities, u_i—uncertainty of an input quantity, Equations (3)–(5) and k—coverage factor.

Both methods of calculating the expanded uncertainty, that is, the MC simulation and the uncertainty propagation method, yielded similar results (see Table 3).

6.2. Heat Transfer Investigation

6.2.1. Main Characteristics

The central mini-channel of the set of five channels in the test section was considered in heat transfer calculations as a model mini-channel. The main aim is to determine local heat transfer coefficients between the heated foil and the working fluid that flows along the channel. The heat transfer coefficient is calculated according to the 2D mathematical method, assuming two directions of heat transfer: one consistent with the depth of the channel and the second consistent with the flow direction. The inverse heat transfer problem in two adjacent domains given by Equations (8)–(11) and the boundary condition presented in Figure 3 was solved by the FEM with Trefftz-type basis functions. The calculation

procedure is described in detail in [22,23]. The results are also illustrated as boiling curves. The error analysis of the results is provided.

6.2.2. The Temperature Measurements and Boiling Curves

Figure 6 shows the temperature of the heated foil measured by an infrared camera as a function of distance from the mini-channel inlet and time. The dependence of heat flux as a function of time for the entire experiment is shown in Figure 7. Data referring to the subcooled boiling region are marked in grey.

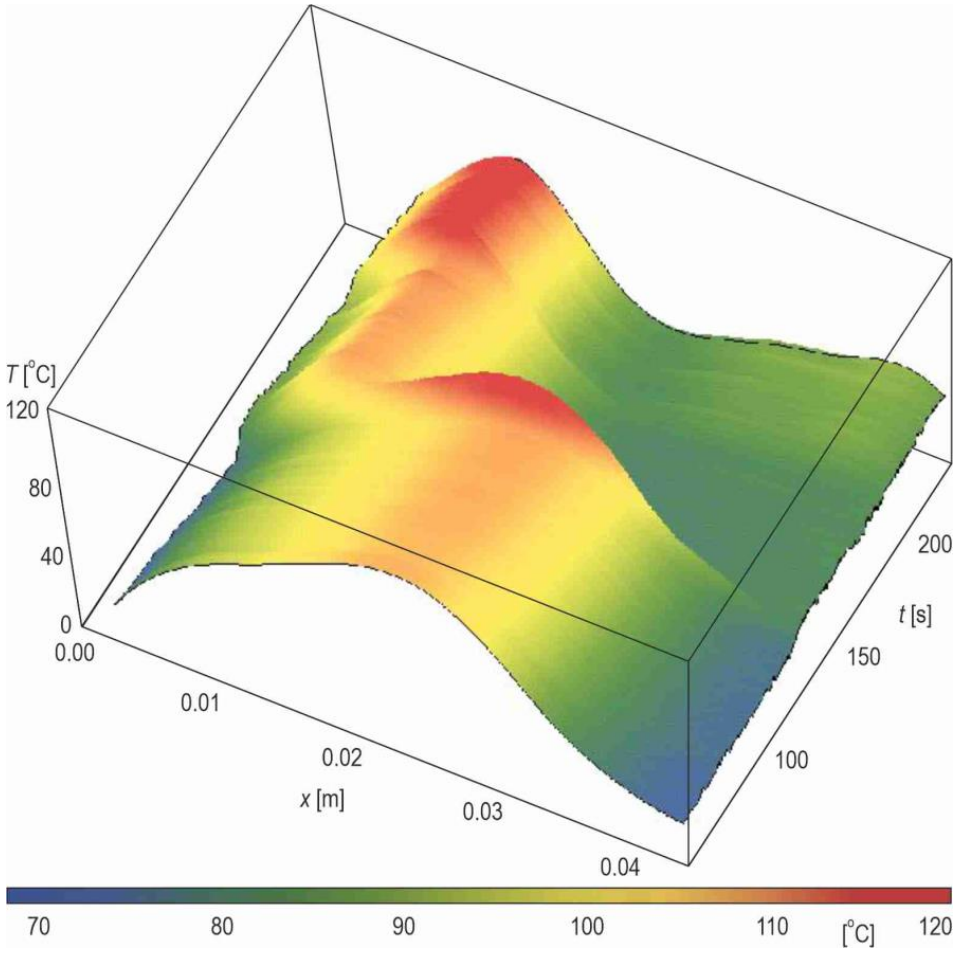

Figure 6. The temperature of the heated foil measured by an infrared camera as a function of distance from the mini-channel inlet and time; the experimental parameters are shown in Table 1.

It should be underlined that the heat flux dependence presented in Figure 7 and the boiling curves shown in Figure 8 were based on data from the entire experimental series. However, Figures 6 and 9–11 refer only to the subcooled boiling region (assumed to be between 72 s and 222 s).

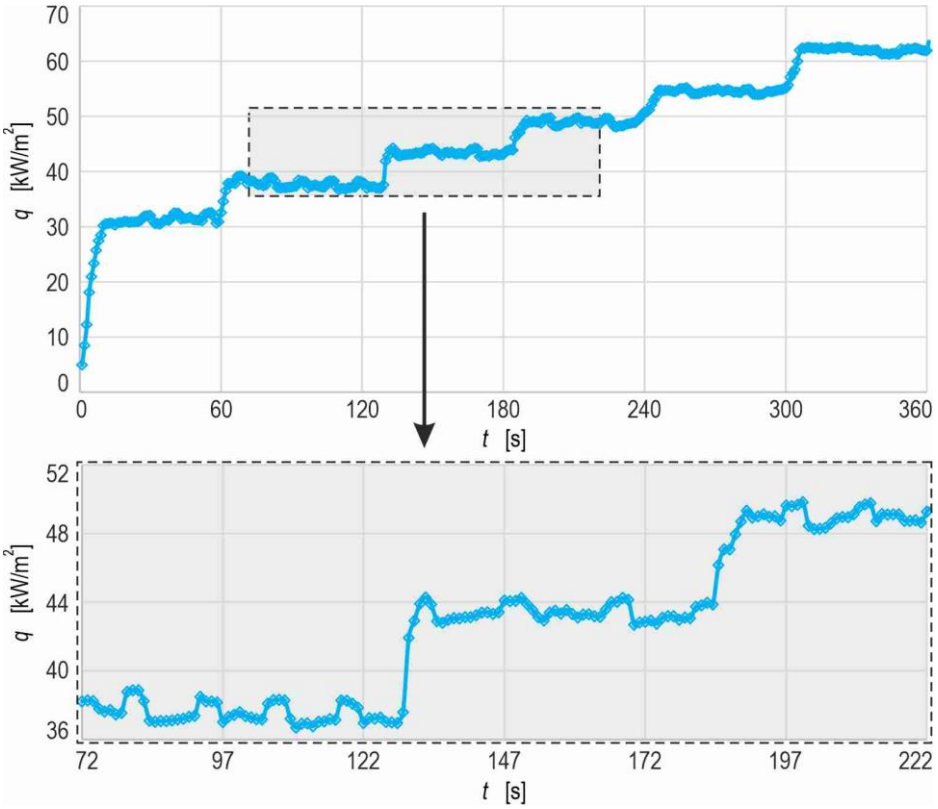

Figure 7. Heat flux supplied to the heated foil as a function of time; the data referring to the subcooled boiling region is marked in grey; the experimental parameters are shown in Table 1.

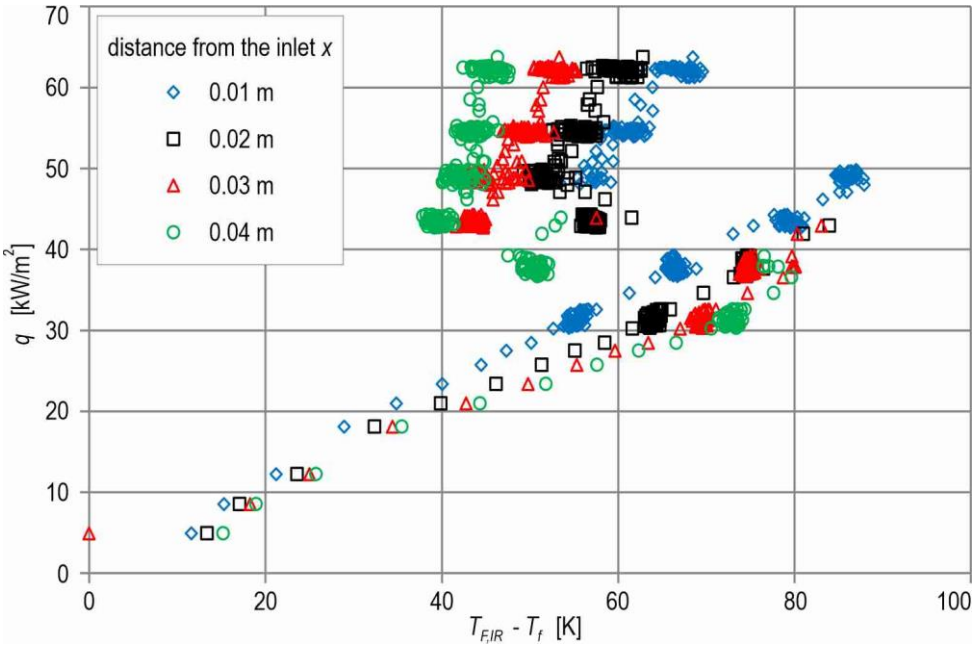

Figure 8. Boiling curves, i.e., the dependences of heat flux as a function of the temperature difference between the heated wall and the bulk fluid temperature, for four distances from the mini-channels inlet; the experimental parameters shown in Table 1.

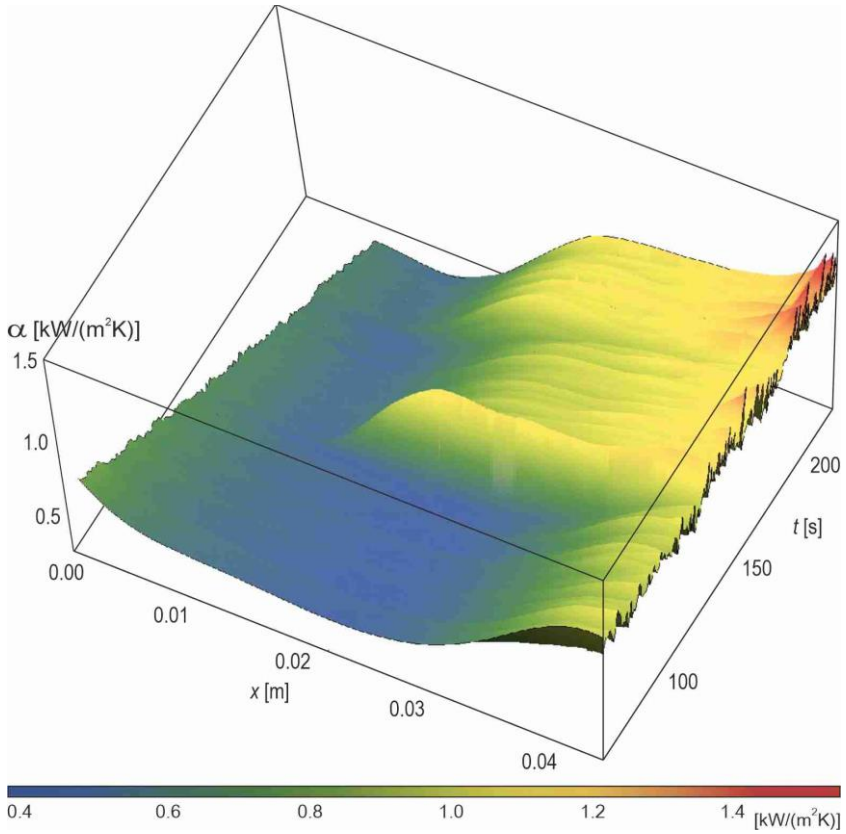

Figure 9. The heat transfer coefficient as a function of distance from the mini-channel inlet and time; the experimental parameters shown in Table 1.

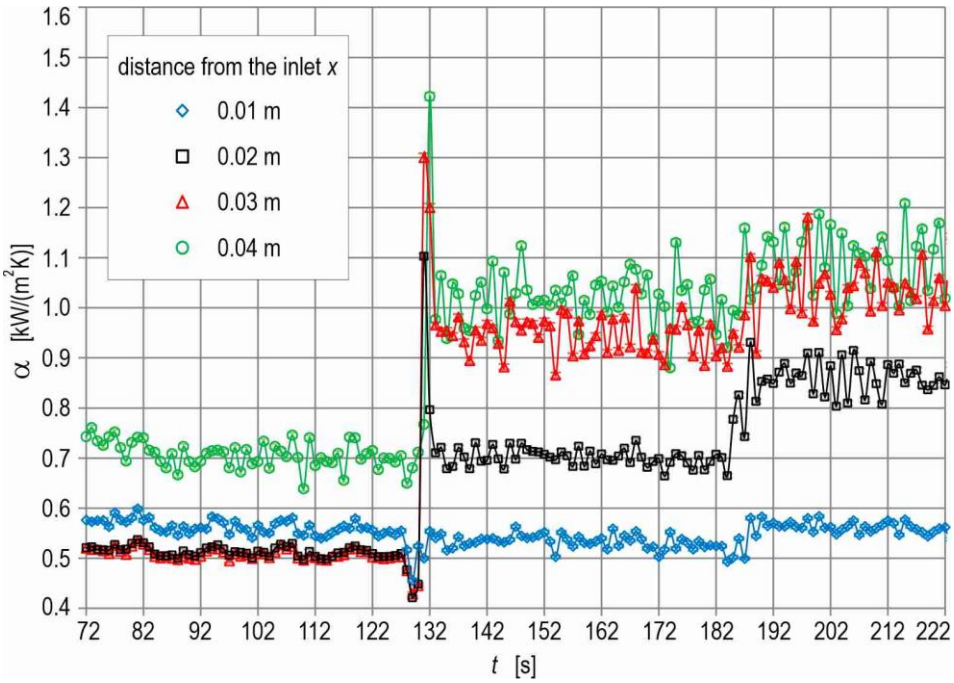

Figure 10. The heat transfer coefficient as a function of time, for four selected distances from the inlet; the subcooled boiling region; and the experimental parameters, as shown in Table 1.

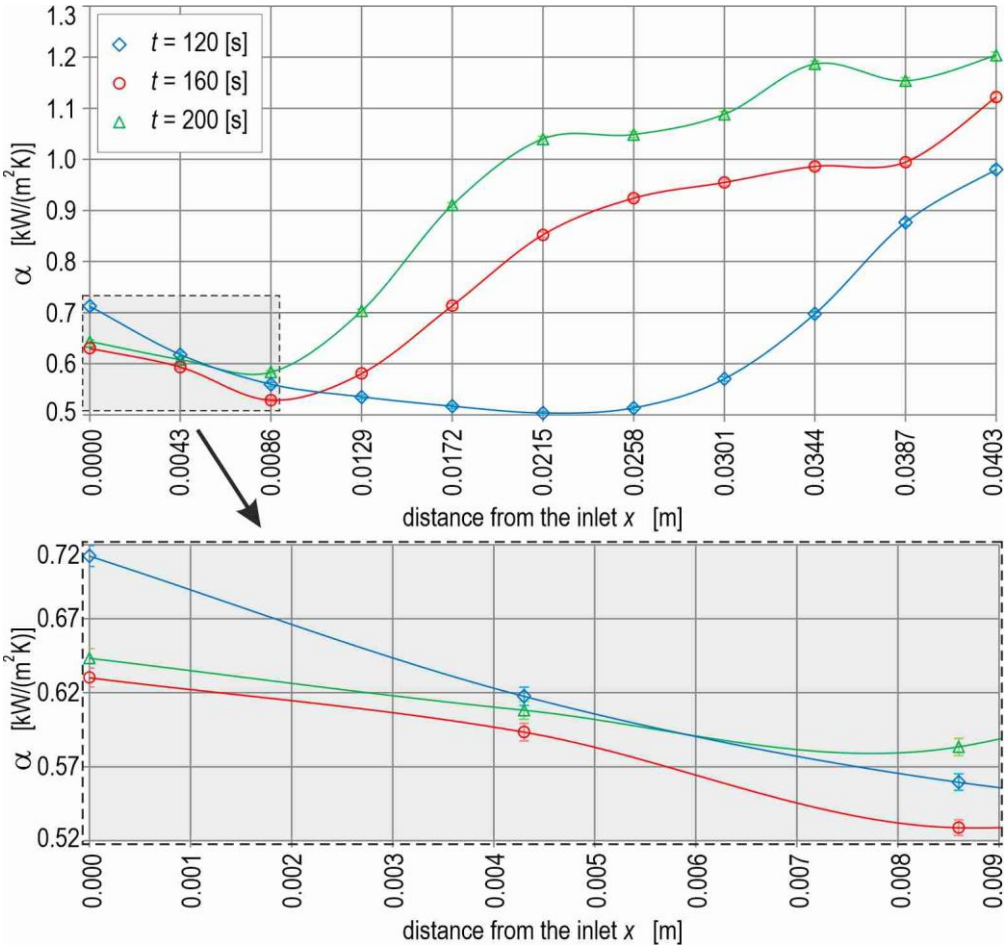

Figure 11. The heat transfer coefficient as a function of distance from the inlet with marked error bars of the heat transfer coefficient, the subcooled boiling region; the results obtained for three selected times and other main experimental parameters shown in Table 1.

According to the data shown in Figure 7, it can be seen that the gradual increase in heat flux corresponded to the stepped heat flux distribution. Marked data, which refer to the subcooled boiling region, were collected for three increasing values of heat flux. This stepped increase in heat flux is particularly recognizable for the approximated time ranges of 128–132 s and 182–192 s.

Figure 8 illustrates the dependences of heat flux as a function of the temperature difference between the heated foil (measured by infrared thermography) and the bulk fluid temperature for the selected points on the mini-channel axis line (known as boiling curves). These points correspond to selected distances from the mini-channel inlet. Four distances were chosen: 0.01 m, 0.02 m, 0.03 m, and 0.04 m.

When analysing the boiling curves shown in Figure 8, it can be seen that all have a typical course characteristic for refrigerants. At the beginning of increasing heat flux, heat transfer between the heated foil and the fluid proceeds by single-phase forced convection. It is visible as an increasing function. The increase in activation of the vapour nuclei on the heated wall and their spontaneous nucleation then cause a temperature drop on the surface as a result of their acting as internal heat sinks. This temperature drop is evidence that 'nucleation hysteresis' occurred. A further increase in the heat flux leads to developed nucleate boiling, visible again as an increasing function. The highest temperature drop occurred for the distance x = 0.01 m. Furthermore, it can be concluded that, in general, with increasing distance from the inlet, the temperature drop accompanying 'nucleation hysteresis' decreases.

6.2.3. The Heat Transfer Coefficient Results

The Trefftz function-based thermal solution of the inverse problem in an unsteady state flow boiling heat transfer in a mini-channel is realized. The method of determining the heat transfer coefficient is described in detail in Section 5. Finally, the local heat transfer coefficients are determined from Equation (7).

The heat transfer coefficient as a function of distance from the inlet and time for the subcooled boiling region is presented in Figure 9.

It should be explained that in the heat transfer calculations, only data from the experiment concerning the subcooled boiling region were considered. The time interval corresponding to this region was found to range between 72 and 222 s. The results shown in Figures 10 and 11 correspond to this time interval.

The local heat transfer coefficients versus time, for four distances from the mini-channel inlet, are presented in Figure 10. Furthermore, the heat transfer coefficient as a function of distance from the inlet obtained for three selected times (120 s, 160 s and 200 s) with marked error bars of the heat transfer coefficient is shown in Figure 11. Additionally, the enlarged part of the graph illustrates the data in a narrower time interval.

Generally, the highest heat transfer coefficients were observed near the outlet and for the last time moments corresponding to the highest heat flux, as shown in Figure 9. However, it should be underlined that for the heat transfer analysis, selected representative dependences of the heat transfer coefficients were chosen: versus time for selected distances from the inlet and versus distance for the selected times of the experiment. The chosen time interval corresponds to three sets of increased heat flux (shown in Figure 7) within the subcooled boiling region (these data are marked in grey).

According to the results presented in Figures 9 and 11, it was noticed that local heat transfer coefficients in the subcooled boiling region increased with distance from the mini-channel inlet in general. Although near the inlet, lower values of the coefficient are gained, and the relationship is a decreasing function of the distance from the inlet up to 0.0086 m. The increasing function is then observed with the maximum values of the local heat transfer coefficients for time t = 200 s (corresponding to the highest heat flux of the three selected values). Furthermore, for the lowest heat flux, corresponding to time t = 120 s, the course of the dependence differs from the others for distances greater than 0.0086 m from the inlet.

When analysing the relationships shown in Figure 10, it is clear that the increase in time, i.e., heat flux during the experiment, caused an increase in the heat transfer coefficient (see Figure 7). Furthermore, when an increase in the heat flux was provided, there was large scatter in the coefficient values. It is seen for time moments in the range of 128–132 s. Slightly lower scatter can be noticed at a time interval of 182–192 s.

6.2.4. The Heat Transfer Coefficient Uncertainty

The mean relative error of the heat transfer coefficient was calculated by the following equation:

$$\varepsilon_\alpha = \frac{\left(\left(\frac{\partial \alpha}{\partial \lambda}\Delta\lambda\right)^2 + \left(\frac{\partial \alpha}{\partial T_F}\Delta T_F\right)^2 + \left(\frac{\partial \alpha}{\partial T_f}\Delta T_f\right)^2 + \left(\frac{\partial \alpha}{\partial\left(\frac{\partial T_F}{\partial y}\right)}\Delta\left(\frac{\partial T_F}{\partial y}\right)\right)^2 \right)^{\frac{1}{2}}}{\alpha(x,y)} \quad (14)$$

where:

$\Delta T_F = \Delta T_{IR} + \left(\left(\frac{\partial T_F}{\partial x}\Delta x\right)^2 + \left(\frac{\partial T_F}{\partial t}\Delta t\right)^2 \right)^{\frac{1}{2}}$—the accuracy of the foil temperature approximation;

$\Delta T_f = \Delta T_{TK} + \left(\left(\frac{\partial T_f}{\partial x}\Delta x\right)^2 + \left(\frac{\partial T_f}{\partial t}\Delta t\right)^2 \right)^{\frac{1}{2}}$—the accuracy of the fluid temperature determination;

$\left(\frac{\partial T_F}{\partial y}\right) = \left(\left(\frac{\partial^2 T_F}{\partial y \partial x}\Delta x\right)^2 + \left(\frac{\partial^2 T_F}{\partial y \partial t}\Delta t\right)^2\right)^{\frac{1}{2}}$ — the accuracy of the derivative of the foil temperature with respect to y;
ΔT_{IR} = 1.97 K—uncertainty of temperature measurement by the infrared camera, assumed as the expanded uncertainty according to the MC simulation U_{MC} (see Table 3);
ΔT_{TK} = 1.48 K—uncertainty of temperature measurement by thermoelements, it was assumed as the expanded uncertainty according to MC simulation U_{MC} (see Table 3);
Δx = 0.000099 m—uncertainty of infrared thermography temperature measurement location;
Δt = 0.01 s — time measurement uncertainty of temperature reading;
$\Delta \lambda$ = 0.1 W/(m·K)—uncertainty of the thermal conductivity of the heated foil material, based on the known temperature and data specified by its manufacturer.

The mean relative error of the heat transfer coefficient ε_α as a function of time is illustrated in Figure 12. The results refer to the time interval corresponding to the subcooled boiling region (time interval between 72 and 222 s).

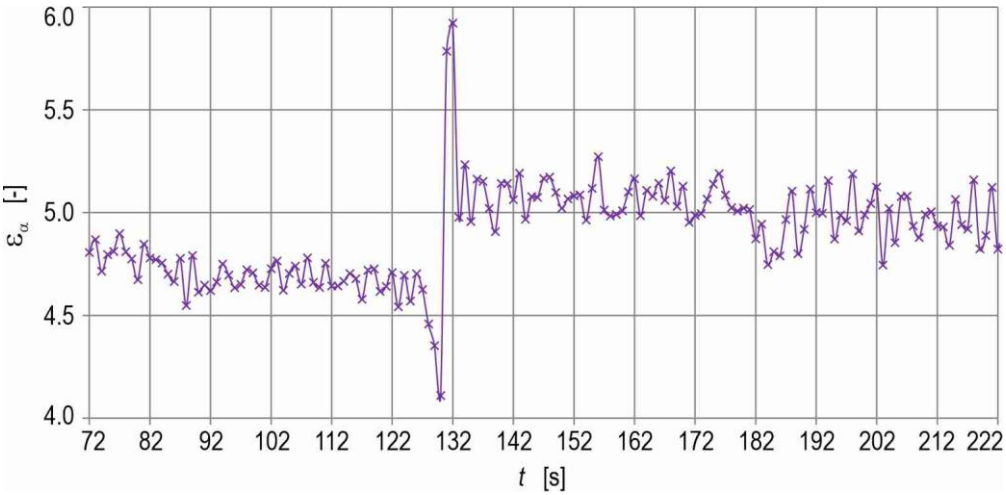

Figure 12. The mean relative error of the heat transfer coefficient as a function of time.

When the mean relative error dependence obtained for the subcooled boiling region is analysed, it can be found that with an increase in time, the mean relative differences increase. It should be added that the data presented in Figure 12 refer to three increases in the heat supplied to the heated foil. Furthermore, the highest relative differences occurred for the time interval corresponding to the first increase in heat flux in the subcooled boiling region. The relative errors of the heat transfer coefficient obtained for the subcooled boiling region were found to be rather low, that is, of the order of a few percent, similarly to [30].

7. Conclusions

This paper focused on heat transfer calculations of flow boiling in mini-channels and estimated the uncertainty of temperature measurement. The investigations involved heat transfer during fluid flow in five parallel mini-channels that constitute a test section with a common heated wall. The heat transfer coefficient was determined from the Robin condition. The foil and fluid temperature distributions were found to be solutions to the inverse heat transfer problem with the aid of the FEM with the Trefftz-type basis functions.

For estimation of temperature measurement uncertainty, the temperature on the heated wall of the mini-channels was measured according to two techniques: the contact method and the contactless method. During the experiment, temperature measurements of the heated wall surface were performed simultaneously with the use of K-type thermoelements (a contact method) and an infrared camera (a contactless method). Statistical analyses were based on the collected temperature data collected. The estimation of the uncertainty of

surface temperature measurement was performed using the Monte Carlo method. The results obtained from this simulation method were compared with the results of the computation related to the uncertainty propagation method. The results of applying both methods were found to be consistent.

Considering heat transfer investigation, it was found that for all data based on the entire experimental set, the highest heat transfer coefficients were achieved near the outlet and for the last time moments corresponding to the highest heat flux. Taking into account the data from the subcooled boiling region, it was observed that, generally, local heat transfer coefficients increased with distance from the mini-channel inlet. Moreover, the increase in time, i.e., the heat flux during the experiment, caused an increase in the heat transfer coefficient. When the mean relative error dependence obtained for the subcooled boiling region was analysed, it was found that with an increase in time, the mean relative errors increased.

Author Contributions: Conceptualization, M.P. and B.M.; Data curation, M.P.; Formal analysis, M.P. and B.M.; Funding acquisition, M.P.; Investigation, M.P. and A.P.; Methodology, M.P. and B.M.; Project administration, M.P.; Software, B.M.; Visualization, A.P.; Writing—original draft, M.P., B.M. and A.P.; Writing—review & editing, M.P., B.M. and A.P. All authors have read and agreed to the published version of the manuscript.

Funding: The research reported in this article was supported by a grant from Poland's Minister of Education and Science through the Poland's Metrology Programme [Polska Metrologia]. Grant Number: PM/SP/0031/2021/1; Funding: 750,000.00 Polish zlotys; Programme budget: 848,200.00 Polish zlotys.

Data Availability Statement: Data sharing is not applicable.

Conflicts of Interest: The authors declare no conflict of interest.

References

1. de Oliveira, J.D.; Copetti, J.B.; Passos, J.C.; van der Geld, C.W.M. On Flow Boiling of R-1270 in a Small Horizontal Tube: Flow Patterns and Heat Transfer. *Appl. Therm. Eng.* **2020**, *178*, 115403. [CrossRef]
2. Piasecka, M.; Strąk, K. Boiling Heat Transfer during Flow in Vertical Mini-Channels with a Modified Heated Surface. *Energies* **2022**, *15*, 7050. [CrossRef]
3. Dąbek, L.; Kapjor, A.; Orman, Ł.J. Boiling Heat Transfer Augmentation on Surfaces Covered with Phosphor Bronze Meshes. *MATEC Web Conf.* **2018**, *168*, 07001. [CrossRef]
4. Dąbek, L.; Kapjor, A.; Orman, Ł.J. Distilled Water and Ethyl Alcohol Boiling Heat Transfer on Selected Meshed Surfaces. *Mech. Ind.* **2019**, *20*, 701. [CrossRef]
5. Kruzel, M.; Bohdal, T.; Sikora, M. Heat Transfer and Pressure Drop during Refrigerants Condensation in Compact Heat Exchangers. *Int. J. Heat Mass Transf.* **2020**, *161*, 120283. [CrossRef]
6. Bohdal, T.; Kruzel, M. Refrigerant Condensation in Vertical Pipe Minichannels under Various Heat Flux Density Level. *Int. J. Heat Mass Transf.* **2020**, *146*, 118849. [CrossRef]
7. Rastan, H.; Abdi, A.; Hamawandi, B.; Ignatowicz, M.; Meyer, J.P.; Palm, B. Heat Transfer Study of Enhanced Additively Manufactured Minichannel Heat Exchangers. *Int. J. Heat Mass Transf.* **2020**, *161*, 120271. [CrossRef]
8. Klugmann, M.; Dabrowski, P.; Mikielewicz, D. Flow Distribution and Heat Transfer in Minigap and Minichannel Heat Exchangers during Flow Boiling. *Appl. Therm. Eng.* **2020**, *181*, 116034. [CrossRef]
9. Grabowski, M.; Hozejowska, S.; Maciejewska, B.; Placzkowski, K.; Poniewski, M.E. Application of the 2-D Trefftz Method for Identification of Flow Boiling Heat Transfer Coefficient in a Rectangular MiniChannel. *Energies* **2020**, *13*, 3973. [CrossRef]
10. Liu, G.; He, C.; Wen, Q.; Wang, Z.; Wang, X.; Shittu, S.; Zhao, X.; Hu, M. Investigation on Visualization and Heat Transfer Performance Study of the Mini-Channel Flow Boiling. *Int. Commun. Heat Mass Transf.* **2022**, *138*, 106360. [CrossRef]
11. Enoki, K.; Ono, M.; Okawa, T.; Kristiawan, B.; Wijayanta, A.T. Water Flow Boiling Heat Transfer in Vertical Minichannel. *Exp. Therm. Fluid Sci.* **2020**, *117*, 110147. [CrossRef]
12. Carlomagno, G.M.; Cardone, G. Infrared Thermography for Convective Heat Transfer Measurements. *Exp. Fluids* **2010**, *49*, 1187–1218. [CrossRef]

13. Poniewski, M.E.; Hożejowska, S.; Kaniowski, R.; Maciejewska, B.; Pastuszko, R.; Piasecka, M.; Wójcik, T.M. *Encyclopedia of Two-Phase Heat Transfer and Flow I: Fundamentals and Methods Volume 4: Special Topics in Pool and Flow Boiling*; Thome, J.R., Ed.; World Scientific: Singapore, 2015; ISBN 978-981-4623-20-9.
14. Piasecka, M.; Piasecki, A.; Dadas, N. Experimental Study and CFD Modeling of Fluid Flow and Heat Transfer Characteristics in a Mini-Channel Heat Sink Using Simcenter STAR-CCM+ Software. *Energies* **2022**, *15*, 536. [CrossRef]
15. Maciejewska, B.; Piasecka, M.; Piasecki, A. The Study of the Onset of Flow Boiling in Minichannels—Time-Dependent Heat Transfer Results. *Heat Transf. Eng.* **2022**, *43*, 223–237. [CrossRef]
16. Shah, N.A.; Wakif, A.; El-Zahar, E.R.; Thumma, T.; Yook, S.-J. Heat Transfers Thermodynamic Activity of a Second-Grade Ternary Nanofluid Flow over a Vertical Plate with Atangana-Baleanu Time-Fractional Integral. *Alexandria Eng. J.* **2022**, *61*, 10045–10053. [CrossRef]
17. Abderrahmane, A.; Qasem, N.A.A.; Younis, O.; Marzouki, R.; Mourad, A.; Shah, N.A.; Chung, J.D. MHD Hybrid Nanofluid Mixed Convection Heat Transfer and Entropy Generation in a 3-D Triangular Porous Cavity with Zigzag Wall and Rotating Cylinder. *Mathematics* **2022**, *10*, 769. [CrossRef]
18. Grabowski, M.; Poniewski, M.E.; Hożejowska, S.; Pawińska, A. Numerical Simulation of the Temperature Fields in a Single-Phase Flow in an Asymmetrically Heated Mininchannel. *J. Eng. Phys. Thermophys.* **2020**, *93*, 355–363. [CrossRef]
19. Zaborowska, I.; Grzybowski, H.; Rafalko, G.; Mosdorf, R. Boiling Dynamics in Parallel Minichannel System with Different Inlet Solutions. *Int. J. Heat Mass Transf.* **2021**, *165*, 120655. [CrossRef]
20. Kuczynski, W.; Bohdal, T.; Meyer, J.P.; Denis, A. A Regressive Model for Dynamic Instabilities during the Condensation of R404A and R507 Refrigerants. *Int. J. Heat Mass Transf.* **2019**, *141*, 1025–1035. [CrossRef]
21. Maciejewska, B. The Application of Beck's Method Combined with FEM and Trefftz Functions to Determine the Heat Transfer Coefficient in a Minichannel. *J. Theor. Appl. Mech.* **2017**, *55*, 103–116. [CrossRef]
22. Maciejewska, B.; Piasecka, M. Trefftz Function-Based Thermal Solution of Inverse Problem in Unsteady-State Flow Boiling Heat Transfer in a Minichannel. *Int. J. Heat Mass Transf.* **2017**, *107*, 925–933. [CrossRef]
23. Maciejewska, B.; Piasecka, M. Time-Dependent Study of Boiling Heat Transfer Coefficient in a Vertical Minichannel. *Int. J. Numer. Methods Heat Fluid Flow* **2019**, *30*, 2953–2969. [CrossRef]
24. Piasecka, M.; Hożejowska, S.; Maciejewska, B.; Pawińska, A. Time-Dependent Heat Transfer Calculations with Trefftz and Picard Methods for Flow Boiling in a Mini-Channel Heat Sink. *Energies* **2021**, *14*, 1832. [CrossRef]
25. Piasecka, M.; Maciejewska, B.; Łabędzki, P. Heat Transfer Coefficient Determination during FC-72 Flow in a Minichannel Heat Sink Using the Trefftz Functions and ADINA Software. *Energies* **2020**, *13*, 6647. [CrossRef]
26. Piasecka, M.; Maciejewska, B.; Łabędzki, P. Development of FEM Calculation Methods to Analyse Subcooled Boiling Heat Transfer in Minichannels Based on Experimental Results. *Appl. Sci.* **2022**, *12*, 12982. [CrossRef]
27. Maciejewska, B.; Błasiak, S.; Piasecka, M. Determination of the Temperature Distribution in a Minichannel Using ANSYS CFX and a Procedure Based on the Trefftz Functions. *EPJ Web Conf.* **2017**, *143*, 02071. [CrossRef]
28. Joint Committee for Guides in Metrology (JCGM/WG 1). *Evaluation of Measurement Data—Supplement 1 to the "Guide to the Expression of Uncertainty in Measurement"—Propagation of Distributions Using a Monte Carlo Method*; Joint Committee for Guides in Metrology (JCGM): Sèvres, France, 2008.
29. Joint Committee for Guides in Metrology (JCGM/WG 1). *Evaluation of Measurement Data—Guide to the Expression of Uncertainty in Measurement*; Joint Committee for Guides in Metrology (JCGM/WG 1): Sèvres, France, 2008.
30. Piasecka, M.; Strąk, K.; Maciejewska, B. Heat Transfer Characteristics during Flow along Horizontal and Vertical Minichannels. *Int. J. Multiph. Flow* **2021**, *137*, 103559. [CrossRef]